AIAA 2013-0614

Modeling of Jet-by-Jet Diffraction

Dimitri Papamoschou*

The paper presents an analytical model for the prediction of jet-by-jet diffraction. The source jet is modeled as a radiating cylinder on which one can prescribe an arbitrary pressure distribution. This treatment enables the incorporation of wavepacket sources that are becoming prominent in the simulation of jet noise. The scattering jet is modeled as an inviscid cylindrical interface with plug flow of variable Mach number and temperature. The ambient Mach number is also variable. The analysis solves the convective wave equation for the incident, scattered, and transmitted fields. To compare with available experiments the prescribed pressure field on the radiating cylinder is parameterized to reproduce the experimental directivity of the far-field intensity of the isolated jet. The results show that scattering by the fluid interface of the jet is a powerful phenomenon of similar magnitude as scattering from a solid cylinder. Regions of attenuation and amplification are identified. Comparison with available experimental data indicates that the model predicts the reduction and amplification trends with good agreement, its fidelity being better than those of past models that used a point source to simulate the jet noise.

Nomenclature

a	=	speed of sound
A	=	wavepacket amplitude function
k	=	acoustic wavenumber = ω/a_∞
k_x	=	axial wavenumber
k_r	=	radial wavenumber
K	=	modified radial wavenumber
M	=	Mach number
n	=	helical mode
p	=	acoustic pressure
r	=	radial distance in polar coordinate system
R	=	cylinder radius
R_o	=	observer distance
S	=	cylinder separation
t	=	time
U	=	velocity
α	=	instability wavenumber
θ	=	polar angle relative to jet axis
ψ	=	azimuth angle
ϕ	=	perturbation velocity potential
ρ	=	density
ω	=	angular frequency

Subscripts

1	=	scattering jet
2	=	source jet
∞	=	freestream
i	=	incident
o	=	observer

*Professor, Department of Mechanical and Aerospace Engineering, Fellow AIAA

s	=	scattered
t	=	transmitted
tot	=	total

Modifiers

$\widehat{(\ )}$	=	axial Fourier transform

I. Introduction

The subject of this study is the diffraction of jet noise by an adjacent jet. Although this phenomenon is usually referred to as "jet-by-jet shielding", this description is not entirely accurate as the interaction between the two jets causes regions of sound attenuation as well zones of amplification. Therefore, the terms jet-by-jet scattering or jet-by-jet diffraction are more accurate.

The investigation of this topic is motivated by the need for higher-fidelity predictions of aircraft noise. As will be shown in this report, the scattering of sound by the jet is as prominent as the scattering from aircraft surfaces. Therefore the phenomenon of jet-by-jet diffraction deserves the same level of attention as propulsion-airframe integration. The situation is particularly relevant to the development of the Hybrid-Wing-Body (HWB) aircraft,[1] a version of which is depicted in Fig. 1. The engines are installed in close proximity to each other and are surrounded by nearby scattering surfaces, including the vertical fins and the elevon. It is anticipated that the scattering prediction for this configuration will be significantly affected by the jet-by-jet diffraction.

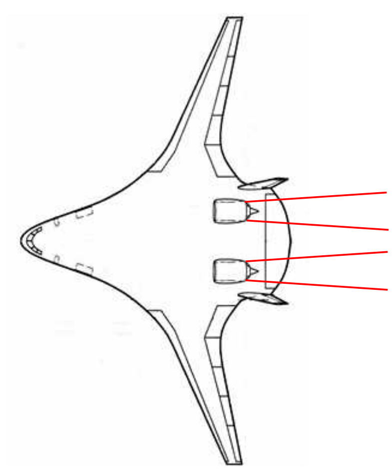

Figure 1. Example of engine layout of Hybrid-Wing-Body airplane (Ref. 2).

Research on jet-by-jet diffraction started in the 1970s. Early experimental by Kantola,[3] Bhat,[4] and Shivashankara and Bhat[5] showed significant noise reduction when one jet "shadows" the other jet. Kantola offered a very simple two-dimensional, plane-wave model for the refraction. Gerhold[6] developed a more advanced model of shielding by considering the diffraction of an infinite line source from an infinite cylindrical fluid interface. His model was thus inherently two-dimensional. Gerhold's model motivated an experimental study by Yu and Fratello[7] on the diffraction by a jet of a point source, simulated by a horn powered by acoustic drivers. An extension of Gerhold's approach to a point quadrupole was performed by Lancey.[8]

The most complete experimental and theoretical work to date is by Simonich, Amiet and Schlinker,[9] hereinafter referred to as SAS. The experiments used two identical jets at a variety of Mach numbers, temperatures, and spacings. The polar and azimuthal emission directions were thoroughly covered. Their study includes an extension of Gerhold's theoretical model to three dimensions by analyzing the diffraction of a monopole point source by a cylindrical plug flow simulating the jet. Their theoretical predictions of changes in the sound pressure level are in fair qualitative agreement with the experiments, although some trends are missed.

This work extends the past theoretical approaches to a source defined by an arbitrary pressure distribution on a cylindrical surface (the radiating cylinder). The setup is illustrated in Fig. 2. This formulation captures the extended nature of the jet noise source and allows the incorporation of wavepacket models that are becoming prominent in the simulation of jet noise. The noise emitted by the radiating cylinder is scattered by a cylindrical fluid interface (the scattering cylinder) with variable Mach number and temperature. The ambient Mach number and temperature are adjustable. An important attribute of this model is that it allows the treatment of non-axisymmetric sources (e.g., spiral modes) that dominate jet noise emission at high frequency. The parameters governing the pressure distribution on the radiating cylinder can be adjusted such as to reproduce the far-field directivity of jet noise, a process that enhances the fidelity of the predictions.

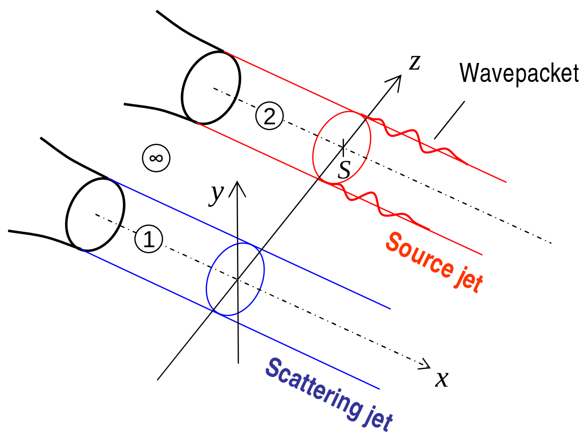

Figure 2. Present treatment of the jet-by-jet scattering problem.

II. Analytical model

The analytical model developed here expands the treatment of SAS to an arbitrary source prescribed on a cylinder. In addition, it allows the flexibility of the freestream Mach number as a variable.

A. Governing Equation

Consider a harmonic field oscillating as $e^{-i\omega t}$ in a uniform flow with Mach number M. The acoustic potential $\phi(x,y,z)$ satisfies the convective wave equation, whose harmonic form is

$$k^2\phi + 2ikM\frac{\partial\phi}{\partial x} + (1-M^2)\frac{\partial^2\phi}{\partial x^2} + \nabla_2^2\phi = 0 \tag{1}$$

where

$$\nabla_2^2\phi \;=\; \frac{\partial^2\phi}{\partial y^2} + \frac{\partial^2\phi}{\partial z^2}$$

and $k = \omega/a_\infty$ is the acoustic wavenumber. Assume that $\phi(x,y,z)$ has a Fourier transform in x, $\widehat{\phi}(k_x,y,z)$, where k_x is the axial wavenumber. The velocity potential is expanded in its spatial Fourier components

$$\phi(x,y,z) \;=\; \frac{1}{2\pi}\int_{-\infty}^{\infty}\widehat{\phi}(k_x,y,z)e^{ik_x x}dk_x \tag{2}$$

It is then easy to show that Eq. 1 reduces to

$$(\nabla_2^2 + K^2)\widehat{\phi} \;=\; 0 \tag{3}$$

where

$$K^2 \;=\; (k - k_x M)^2 - k_x^2 \tag{4}$$

is the transformed lateral wavenumber (or the transformed radial wavenumber in cylindrical coordinates). The governing equation for $\widehat{\phi}$ thus reduces to the Hemholtz equation in terms of the transformed wavenumber. Consider now the cylindrical coordinate system (x, r, ψ), with x the axial coordinate, r the radial coordinate, and ψ the azimuthal angle. In this coordinate system Eq. 3 becomes

$$\frac{1}{r}\frac{\partial}{\partial r}\left(r\frac{\partial\widehat{\phi}}{\partial r}\right)+\frac{1}{r^2}\frac{\partial^2\widehat{\phi}}{\partial\psi^2}+K^2\widehat{\phi}=0 \tag{5}$$

The general solution of Eq. 5 takes the following forms for outgoing and internal waves, respectively:

$$\widehat{\phi}(k_x, r, \psi) = \sum_{m=-\infty}^{\infty} A_m H_m^{(1)}(Kr)e^{im\psi} \tag{6}$$

$$\widehat{\phi}(k_x, r, \psi) = \sum_{m=-\infty}^{\infty} B_m J_m(Kr)e^{im\psi} \tag{7}$$

Here $H_m^{(1)}$ is the Hankel function of the first kind of order m, and J_m is the Bessel function of order m. These general solutions will now be applied to the problem of scattering from and transmission through a cylindrical medium; and the problem of radiation from a cylindrical source.

B. Scattered and Transmitted Fields

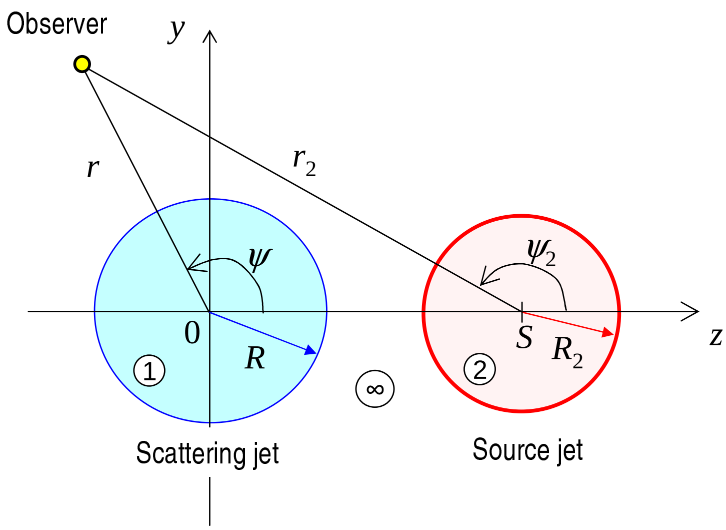

Figure 3. Cross section with definitions of geometric variables.

Referring to Fig. 3, we consider an incident field propagating through an ambient medium having speed of sound a_∞, density ρ_∞ and Mach number M_∞. The incident field interacts with a cylindrical medium centered at the origin of the polar coordinate system and having speed of sound a_1, density ρ_1, and Mach number M_1. The interaction creates a scattered field $\widehat{\phi}_s$ that propagates outward, and a transmitted field $\widehat{\phi}_t$ that propagates inside the cylindrical medium. The general solutions for the scattered and transmitted waves are:

$$\widehat{\phi}_s(k_x, r, \psi) = \sum_{m=-\infty}^{\infty} A_m H_m^{(1)}(K_\infty r)e^{im\psi} \tag{8}$$

$$\widehat{\phi}_t(k_x, r, \psi) = \sum_{m=-\infty}^{\infty} B_m J_m(K_1 r)e^{im\psi} \tag{9}$$

with K defined by Eq. 4.

C. Incident Field

The incident field is radiated from a cylinder centered at $z = S$ and is thus offset from the scattering cylinder. First we develop the solution in the coordinate system of the radiating cylinder. Then we apply a transformation to express the solution in the coordinate system of the scattering cylinder.

1. *Incident field in its own coordinate system*

With respect to the coordinate system (x, r_2, ψ_2) of the radiating cylinder, the incident field

$$\widehat{\phi}_i(k_x, r_2, \psi_2) = \sum_{m=-\infty}^{\infty} C_m H_m^{(1)}(K_\infty r_2) e^{im\psi_2} \tag{10}$$

On the surface of the radiating cylinder, $r_2 = R_2$, we prescribe an acoustic potential $\phi_i(x, R_2, \psi_2)$. Its spatial Fourier components are $\widehat{\phi}_i(k_x, R_2, \psi_2)$, and each component can be expanded in the azimuthal Fourier series,

$$\widehat{\phi}_i(k_x, R_2, \psi_2) = \sum_{m=-\infty}^{\infty} P_m(k_x) e^{im\psi_2} \tag{11}$$

Equation 11 constitutes the boundary condition that must be satisfied by Eq. 10 at $r_2 = R_2$. Application of this boundary condition leads to

$$\widehat{\phi}_i(k_x, r_2, \psi_2) = \sum_{m=-\infty}^{\infty} P_m(k_x) \frac{H_m^{(1)}(K_\infty r_2)}{H_m^{(1)}(K_\infty R_2)} e^{im\psi_2} \tag{12}$$

The solution in the physical domain is

$$\phi_i(x, r_2, \psi_2) = \sum_{m=-\infty}^{\infty} \int_{-\infty}^{\infty} P_m(k_x) \frac{H_m^{(1)}(K_\infty r_2)}{H_m^{(1)}(K_\infty R_2)} e^{im\psi_2} e^{ik_x x} dk_x \tag{13}$$

Consider the special case

$$\phi(x, R_2, \psi_2) = \phi_0(x) e^{in\psi_2} \tag{14}$$

It represents an acoustic potential with axial distribution $\phi_0(x)$ and a helical oscillation with azimuthal mode n. Clearly, in the summation of Eq. 12 only the $m = n$ term is non-zero. The result for the incident field is

$$\widehat{\phi}_i(k_x, r_2, \psi_2) = \widehat{\phi}_0(k_x) \frac{H_n^{(1)}(K_\infty r_2)}{H_n^{(1)}(K_\infty R_2)} e^{in\psi_2} \tag{15}$$

In the analysis that follows we will use this special case. It is straightforward to then generalize the solution to an arbitrary prescribed field on the cylinder. When conducting the analysis for a specific k_x, for simplicity we set $\widehat{\phi}_0(k_x) = 1$, thus the incident field is

$$\widehat{\phi}_i(k_x, r_2, \psi_2) = \frac{H_n^{(1)}(K_\infty r_2)}{H_n^{(1)}(K_\infty R_2)} e^{in\psi_2} \tag{16}$$

2. *Incident field in coordinate system of scattering cylinder*

The solution for the incident field in the coordinate system of the radiating cylinder is not amenable to combining with the solutions for the scattered and transmitted fields, Eqs. 8 and 9. To transform the incident field to the coordinate system (r, ψ) of the scattering cylinder, we use Graf's addition theorem.[10] Refer to Fig. 3. For a Hankel function in the coordinate system (r_2, ψ_2), the addition theorem gives

$$e^{in\psi_2} H_n^{(1)}(kr_2) = \begin{cases} \sum_{m=-\infty}^{\infty} J_{m-n}(kS)\ H_m^{(1)}(kr)\ e^{im\psi}, & r > S \\ \sum_{m=-\infty}^{\infty} J_m(kr)\ H_{m-n}^{(1)}(kS)\ e^{im\psi}, & r < S \end{cases} \tag{17}$$

Application to the incident field of Eq. 16 gives

$$\widehat{\phi}_i(k_x, r, \psi) = \frac{1}{H_n^{(1)}(K_\infty R_2)} \begin{cases} \sum_{m=-\infty}^{\infty} J_{m-n}(K_\infty S)\ H_m^{(1)}(K_\infty r)\ e^{im\psi}, & r > S \\ \sum_{m=-\infty}^{\infty} J_m(K_\infty r)\ H_{m-n}^{(1)}(K_\infty S)\ e^{im\psi}, & r < S \end{cases} \tag{18}$$

Equation 18 is useful for applying the boundary conditions on the surface of the scattered cylinder $r = R$. By definition $R < S$ (the two cylinders cannot overlap) so the near-field version of Eq. 18 ($r < S$) is used.

D. Boundary Conditions

The Fourier coefficients A_m and B_m for the scattered and transmitted fields are determined from the pressure and kinematic boundary conditions on the surface $r = R$ of the scattering cylinder.

1. *Pressure boundary condition*

The pressure field is given by the linearized momentum equation,

$$p \;=\; -\rho\frac{D\phi}{Dt} \;=\; -\rho\left(\frac{\partial}{\partial t}+U\frac{\partial}{\partial x}\right)\phi \tag{19}$$

The spatial Fourier components of a harmonic field satisfy

$$\widehat{p} \;=\; i\rho a(k-k_xM)\widehat{\phi} \tag{20}$$

Pressure equality on the surface of the cylinder requires

$$\widehat{p}_i+\widehat{p}_s \;=\widehat{p}_t \tag{21}$$

or

$$\rho_\infty a_\infty(k_\infty-k_xM_\infty)(\widehat{\phi}_i+\widehat{\phi}_s) \;=\; \rho_1 a_1(k_1-k_xM_1)\widehat{\phi}_t \tag{22}$$

Substituting Eqs. 18, 8, and 9 for the incident, scattered, and transmitted fields, respectively, and matching on a term by term basis,

$$\frac{J_m(K_\infty R)H^{(1)}_{m-n}(K_\infty S)}{H^{(1)}_n(K_\infty R_2)}+A_mH^{(1)}_m(K_\infty R) \;=\; B_m\frac{\rho_1a_1(k_1-k_xM_1)}{\rho_\infty a_\infty(k_\infty-k_xM_\infty)}J_m(K_1R) \tag{23}$$

2. *Kinematic condition at interface*

At a given frequency ω and axial wavenumber k_x the surface of the scattering cylinder (i.e. the interface between the jet and the ambient) undergoes a small perturbation of the form

$$\eta(x,t)=\epsilon e^{i(k_xx-\omega t)} \tag{24}$$

The transverse velocity of the interface is

$$\frac{D\eta}{Dt} \;=\left(\frac{\partial}{\partial t}+U\frac{\partial}{\partial x}\right)\eta \;=\; -i\epsilon a(k-k_xM)e^{i(k_xx-\omega t)} \tag{25}$$

This velocity must be matched by the radial velocity $\partial\phi/\partial r$ of the acoustic fields on either side of the interface. On the outer side ($r = R+$),

$$\frac{\partial}{\partial r}\left(\widehat{\phi}_i+\widehat{\phi}_s\right) \;=\; -i\epsilon a_\infty(k_\infty-k_xM_\infty) \tag{26}$$

On the inner side ($r = R-$),

$$\frac{\partial\widehat{\phi}_t}{\partial r} \;=\; -i\epsilon a_1(k_1-k_xM_1) \tag{27}$$

Setting equal Eqs. 26 and 27,

$$\frac{\partial}{\partial r}\left(\widehat{\phi}_i+\widehat{\phi}_s\right) \;=\; \frac{a_\infty(k_\infty-k_xM_\infty)}{a_1(k_1-k_xM_1)}\;\frac{\partial\widehat{\phi}_t}{\partial r} \tag{28}$$

Inserting Eqs. 18, 8, and 9, and matching terms,

$$\frac{J'_m(K_\infty R)H^{(1)}_{m-n}(K_\infty S)}{H^{(1)}_n(K_\infty R_2)}+A_m{H'}^{(1)}_m(K_\infty R) \;=\; B_m\frac{a_\infty K_1(k_\infty-k_xM_\infty)}{a_1K_\infty(k_1-k_xM_1)}J'_m(K_1R) \tag{29}$$

where $()'$ denotes differentiation with respect to the argument. The relation $J'_m(z) = (m/z)J_m(z) - J_{m+1}(z)$ and the analogous relation for the Hankel function are used to evaluate the derivatives. Equations 23 and 29 are solved simultaneously to yield the Fourier coefficients A_m and B_m.

E. Construction of Solution in Physical Space

Once the coefficients A_m and B_m are determined by the boundary conditions, the resulting solutions of Eqs. 8 and 9 give the scattered and transmitted potential fields for a unit-amplitude potential incident field given by Eq. 16 (or 18). Using Eq. 20 the corresponding pressure fields are:

$$\begin{aligned}\widehat{p}_i &= i\rho_\infty a_\infty(k_\infty - k_x M_\infty)\widehat{\phi}_i \\ \widehat{p}_s &= i\rho_\infty a_\infty(k_\infty - k_x M_\infty)\widehat{\phi}_s \\ \widehat{p}_t &= i\rho_1 a_1(k_1 - k_x M_1)\widehat{\phi}_t\end{aligned} \tag{30}$$

It is clear from Eq. 15 that these pressure fields correspond to a unit-amplitude pressure incident field, i.e., $\widehat{p}_0(k_x) = 1$. For a prescribed field $p_0(x)e^{in\psi_2}$ we simply scale the solutions by the Fourier coefficients $\widehat{p}_0(k_x)$ and integrate over all the axial wavenumbers:

$$\begin{aligned}p_i(x, r_2, \psi_2) &= e^{in\psi_2}\frac{1}{2\pi}\int_{-\infty}^{\infty}\widehat{p}_0(k_x)\frac{H_n^{(1)}(K_\infty r_2)}{H_n^{(1)}(K_\infty R_2)}e^{ik_x x}dk_x \\ p_s(x, r, \psi) &= \frac{1}{2\pi}\int_{-\infty}^{\infty}\widehat{p}_0(k_x)\widehat{p}_s(k_x, r, \psi)e^{ik_x x}dk_x \\ p_t(x, r, \psi) &= \frac{1}{2\pi}\int_{-\infty}^{\infty}\widehat{p}_0(k_x)\widehat{p}_t(k_x, r, \psi)e^{ik_x x}dk_x\end{aligned} \tag{31}$$

For the incident field we use the solution in its own coordinate system (r_2, ψ_2) because the transformation of Eq. 18 is computationally more demanding and exhibits numerical problems at $r = S$. Once the solution is determined in the (r_2, ψ_2) system it is straight-forward to translate it to the (r, ψ) system.

The transmitted field is valid only within the scattering jet, $r < R$. The incident and scattered solutions are not valid within the scattering jet ($r < R$) or within the source jet ($r_2 < R_2$). Outside the source and scattering jets, the total field is the complex summation of the incident and scattered fields:

$$p_{tot}(x, r, \psi) = p_i(x, r, \psi) + p_s(x, r, \psi) \tag{32}$$

F. Evaluation of Intensity Field

To provide realistic predictions of the difference in the sound pressure level due to the interaction of the radiated field with the scattering jet, we must treat the two jets as both radiators and scatterers. Refer to the two jets as Jet 1 and Jet 2. An observer outside those jets will measure the total field (incident plus scattered) with Jet 2 acting as radiator and Jet 1 acting as scatterer (first interaction); and the total field with Jet 1 acting as radiator and Jet 2 acting as scatterer (second interaction). This addition is incoherent because the radiated fields are expected to be uncorrelated. Therefore, we sum the intensities $|p|^2$ of each interaction. The interactions are illustrated in Fig. 4. The top row summarizes the above statement, with red and blue indicating the radiating and scattering jets, respectively. The second row "flips" the coordinate system of the second interaction so that it is in line with the preceding analysis. Accordingly, the intensity measured by the observer is

$$|p(x, y, z)|^2 = |p_{2,i}(x, y, z) + p_{2,s}(x, y, z)|^2 + |p_{1,i}(x, y, S - z) + p_{1,s}(x, y, S - z)|^2 \tag{33}$$

To assess the effect of jet-by-jet scattering we compare the above intensity with the sum of the incident intensities of the isolated jets. Accordingly, we define the change in sound pressure level as

$$\Delta\text{SPL} = 10\log_{10}\left(\frac{|p(x, y, z)|^2}{|p_{2,i}(x, y, z)|^2 + |p_{1,i}(x, y, S - z)|^2}\right) \tag{34}$$

Evaluation of ΔSPL, and comparison with experimental data, uses the spherical coordinate system R_o, θ_o, ψ_o shown in Fig. 5. The system is centered with the axis of Jet 1. For convenience, the observer polar angle is defined to be $\psi_o = 0$ in the downward vertical direction, so it differs from the definition used earlier in the analysis.

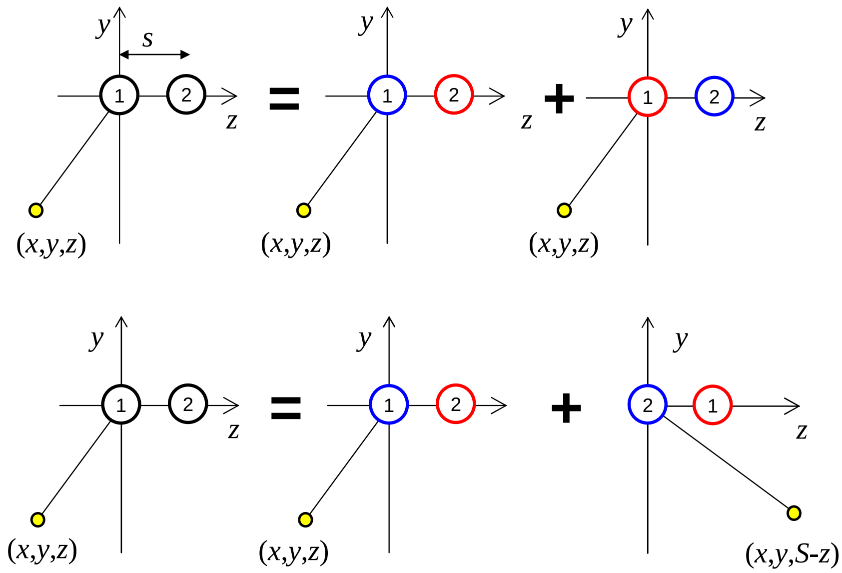

$$|\,p(x,y,z)\,|^2 = \left|p_{2,i}(x,y,z) + p_{2,s}(x,y,z)\right|^2 + \left|p_{1,i}(x,y,S-z) + p_{1,s}(x,y,S-z)\right|^2$$

Figure 4. Interactions between the two jets. Red color indicates radiator, blue color indicates scatterer.

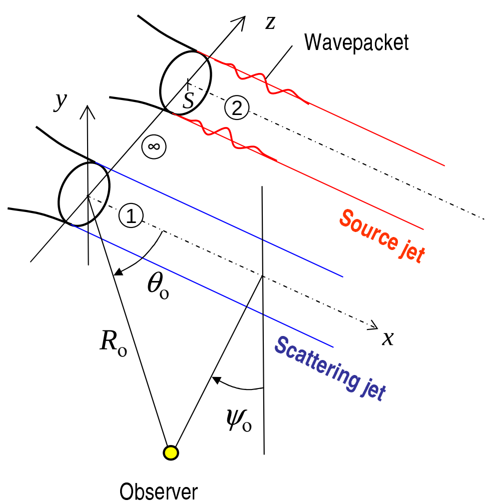

Figure 5. Spherical coordinate system for observer.

III. Source Fields

The present formulation of the scattering problem allows an arbitrary source distribution on the radiating cylinder. In turn, this allows the investigation of a large range of problems, with the cylinder essentially acting as a Kirchhoff surface. The approach can be extended to volume sources inside the cylinder by propagating their sound to the cylinder surface. In this study we focus on the wavepacket surface source, which is of increasing interest in the modeling jet noise. We also cover the treatment of a monopole source that is sometimes combined incoherently with the wavepacket to reproduce to acoustic intensity in the far field.

A. Wavepacket Source

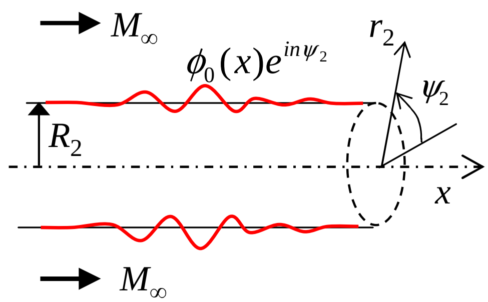

Figure 6. Wavepacket source

The wavepacket source is an amplitude-modulated travelling wave that represents the growth and decay of an instability wave at a fixed frequency. The wavepacket model builds on the foundational works by Tam and Burton,[11] Crighton and Huerre,[12] Avital et al.[13] and Morris.[14] There is increasing experimental evidence that the peak noise radiation is caused by an instability-wave mechanism, as evidenced by a number of near-field experiments, for example the works of Reba et al.[15] In its most general form, the wavepacket is represented by the Fourier series expansion of Eq. 13. Here for simplicity we consider a single azimuthal mode n. The amplitude-modulated traveling and spinning wave, prescribed on the cylinder surface $r_2 = R_2$ (Fig. 6), is represented by

$$p_0(x)e^{in\psi_2} = A(x)e^{i\alpha x}e^{in\psi_2} \tag{35}$$

Here $A(x)$ is the amplification-decay envelope; α is the instability wavenumber; and n is the azimuthal (helical) mode. The convective velocity of the instability wave is

$$U_c = \frac{\omega}{\alpha} \tag{36}$$

and the convective Mach number is

$$M_c = \frac{\omega}{a_\infty \alpha} = \frac{k_\infty}{\alpha} \tag{37}$$

The fraction of the acoustic energy that radiates to the far field increases with increasing M_c and reducing extent of the amplification-decay envelope. For fixed M_c and $A(x)$, the far-field emission weakens with increasing azimuthal mode. Using the pressure analogue of Eq. 15, the solution in wavenumber space is

$$\widehat{p}_i(k_x, r_2, \psi_2) = \widehat{A}(k_x - \alpha)\frac{H_n^{(1)}(K_\infty r_2)}{H_n^{(1)}(K_\infty R_2)}e^{in\psi_2} \tag{38}$$

and the solution in physical space is

$$p_i(x, r_2, \psi_2) = \frac{1}{2\pi}e^{in\psi_2}\int_{-\infty}^{\infty}\widehat{A}(k_x - \alpha)\frac{H_n^{(1)}(K_\infty r_2)}{H_n^{(1)}(K_\infty R_2)}e^{ik_x x}dk_x \tag{39}$$

The wavepacket source can be parameterized based on the polar distribution of the far-field intensity. Using the method of stationary phase, the far-field approximation for the intensity is[16]

$$
\begin{aligned}
|p_i|^2(R_o,\theta_o) &= \frac{1}{(\pi R*)^2}\left|\frac{\widehat{A}\left(\frac{k_\infty(\cos\widetilde{\theta}-M_\infty)}{1-M_\infty^2}-\alpha\right)}{H_n^{(1)}\left(\frac{k_\infty}{\sqrt{1-M_\infty^2}}R_2\sin\widetilde{\theta}\right)}\right|^2 \\
R* &= R_o(\sqrt{1-M_\infty\sin^2\theta_o}) \\
\widetilde{\theta} &= \arctan\left(\sqrt{1-M_\infty^2}\ \tan\theta_o\right)
\end{aligned}
\tag{40}
$$

When the ambient medium is static ($M_\infty = 0$), Eq. 40 reduces to

$$
|p_i|^2(R_o,\theta_o) = \frac{1}{(\pi R_o)^2}\left|\frac{\widehat{A}(k_\infty\cos\theta_o-\alpha)}{H_n^{(1)}(k_\infty R_2\cos\theta_o)}\right|^2 \tag{41}
$$

B. Monopole Source

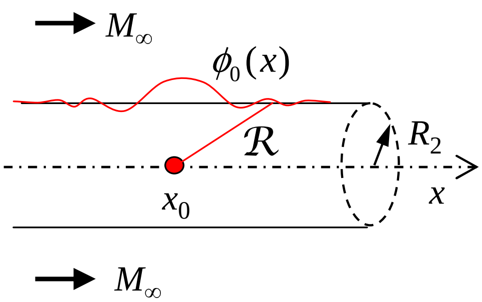

Figure 7. Monopole source,

We examine an acoustic monopole with strength Q located on the centerline of the source cylinder at $x = x_0$ (Fig. 7). Even though the methods developed in this report involve surface sources, the point source problem can be addressed by using the surface pressure distribution on the cylinder $r = R_2$ generated by this source. The acoustic potential field of the monopole is[16]

$$
\begin{aligned}
\phi(x,y,z) &= Q\frac{e^{ik_\infty R'}}{4\pi R^*} \\
R' &= \frac{1}{1-M_\infty^2}\left[R^*-M_\infty(x-x_0)\right] \\
R^* &= \sqrt{(x-x_0)^2+(1-M_\infty^2)(y^2+(z-S)^2)}
\end{aligned}
\tag{42}
$$

On the surface of the cylinder $r_2 = R_2$ we have

$$
\begin{aligned}
\phi_0(x) &= Q\frac{e^{ik_\infty R'}}{4\pi R^*} \\
R' &= \frac{1}{1-M_\infty^2}\left[R^*-M_\infty(x-x_0)\right] \\
R^* &= \sqrt{(x-x_0)^2+(1-M_\infty^2)R_2^2}
\end{aligned}
\tag{43}
$$

This surface distribution can be used in the analytical model of Section II. For a static medium (M_∞=0), $R' = R^* = \mathcal{R}$ where $\mathcal{R}$ is the physical distance between the monopole and a point on the cylinder surface. Consequently Eq. 43 reduces to

$$
\phi_0(x) = Q\frac{e^{ik_\infty\sqrt{R_2^2+(x-x_0)^2}}}{4\pi\sqrt{R_2^2+x^2}} \tag{44}
$$

The far-field intensity can be shown to be[16]

$$|p|^2(R_o,\theta_o) \;=\; Q^2\frac{\rho_\infty^2 a_\infty^2 k_\infty^2}{16\pi^2 R_o^2}\frac{1}{(1-M_\infty^2)^2}\frac{1}{1-M_\infty^2\sin^2\theta_o}\left[1-M_\infty\frac{\cos\theta_o}{\sqrt{1-M_\infty^2\sin^2\theta_o}}\right]^2 \tag{45}$$

and for a static medium becomes

$$|p|^2(R_o) \;=\; Q^2\frac{\rho_\infty^2 a_\infty^2 k_\infty^2}{16\pi^2 R_o^2} \tag{46}$$

C. Source Parameterization

In recent works the jet noise source was simulated by the incoherent superposition of a wavepacket and monopole.[17,18] Referring to Eq. 35, the wavepacket envelope $A(x)$ is expressed in a parametric functional form. An example of such function is

$$A(x) \;=\; \tanh\left(\frac{x}{b_1}\right)^{p_1}\left[1-\tanh\left(\frac{x}{b_2}\right)^{p_2}\right] \tag{47}$$

The amplification part is controlled by the width b_1 and power p_1. The decay part is governed by the width b_2 and power p_2. These constants, together with the instability wavenumber α and monopole strength Q comprise a set of parameters for the noise source. For a given frequency, these parameters are determined by matching the far-field polar intensity distribution using the methods described in Papamoschou.[17] It should be noted that the monopole is very weak and affects only the upstream direction. Example parameterizations will be provided in Section IV.B.

IV. Results

The results are divided in three parts. First we examine the behavior of the pressure field in the cross-sectional plane of Fig. 3 for a fixed axial wavenumber k_x. Then we use realistic source distributions to predict the ΔSPL in the coordinate system of Fig. 5 and compare with available experimental data. Finally we make some predictions for the jet-by-jet diffraction for jets with Mach numbers and spacing similar to the HWB configuration.

A. Diffraction Patterns for Fixed Axial Wavenumber

We study an example with acoustic wavenumber $k = 7.3$; axial wavenumber $k_x = 1$; $R_1 = R_2 = R$; $S/R = 6$; M_1=0.8; $a_1/a_\infty = 1.1$, $M_\infty = 0$; and $n = 2$. The relevant pressure fields are presented in Fig. 8 as contour plots on the $z-y$ plane. Figure 8a shows the spiralling nature of the incident field. The scattered and transmitted fields are shown in Figs. 8b and 8c, respectively. The total field (the addition of scattered and incident fields) is shown in Fig. 8d. The sound attenuation in the "shadow zone" is evident. Figure 8e shows a composite of all the fields (total field outside the cylinders, transmitted field inside the scattering cylinder). To visualize the change in the sound intensity, Fig. 8f plots the ratio of the intensities of the total field and incident field. We observe deep reductions, up to 15 dB, in the shadow zone and moderate amplification at the edge of the shadow zone. The reductions come mainly from the "shielding" effect, but destructive interference also plays a role. The amplification is caused by the reflection of sound from the surface of the scattering cylinder. Constructive interference may also contribute to the amplification. Figure 8f illustrates that scattering by the jet column can be as powerful as scattering by a solid cylinder.

To explore the impact of certain parameters on the diffraction, and illustrate the capability of the method developed, we present in Fig. 9 a "matrix" of pressure fields with varying ambient Mach number M_∞ and azimuthal mode n. The conditions are otherwise the same as in Fig. 8. Increasing the ambient Mach number results in a modest attenuation of the strength of the diffraction pattern. With increasing azimuthal mode the diffraction pattern turns counter-clockwise, consistent with the spiralling motion of the incident waves. We need to keep in mind that in an unforced jet the modes $+n$ and $-n$ have equal likelihood and are presumed to be uncorrelated. Therefore, a complete treatment should compute the diffraction for modes $+n$ and $-n$, then add the solutions incoherently (this means addition of the intensities, not the complex amplitudes).

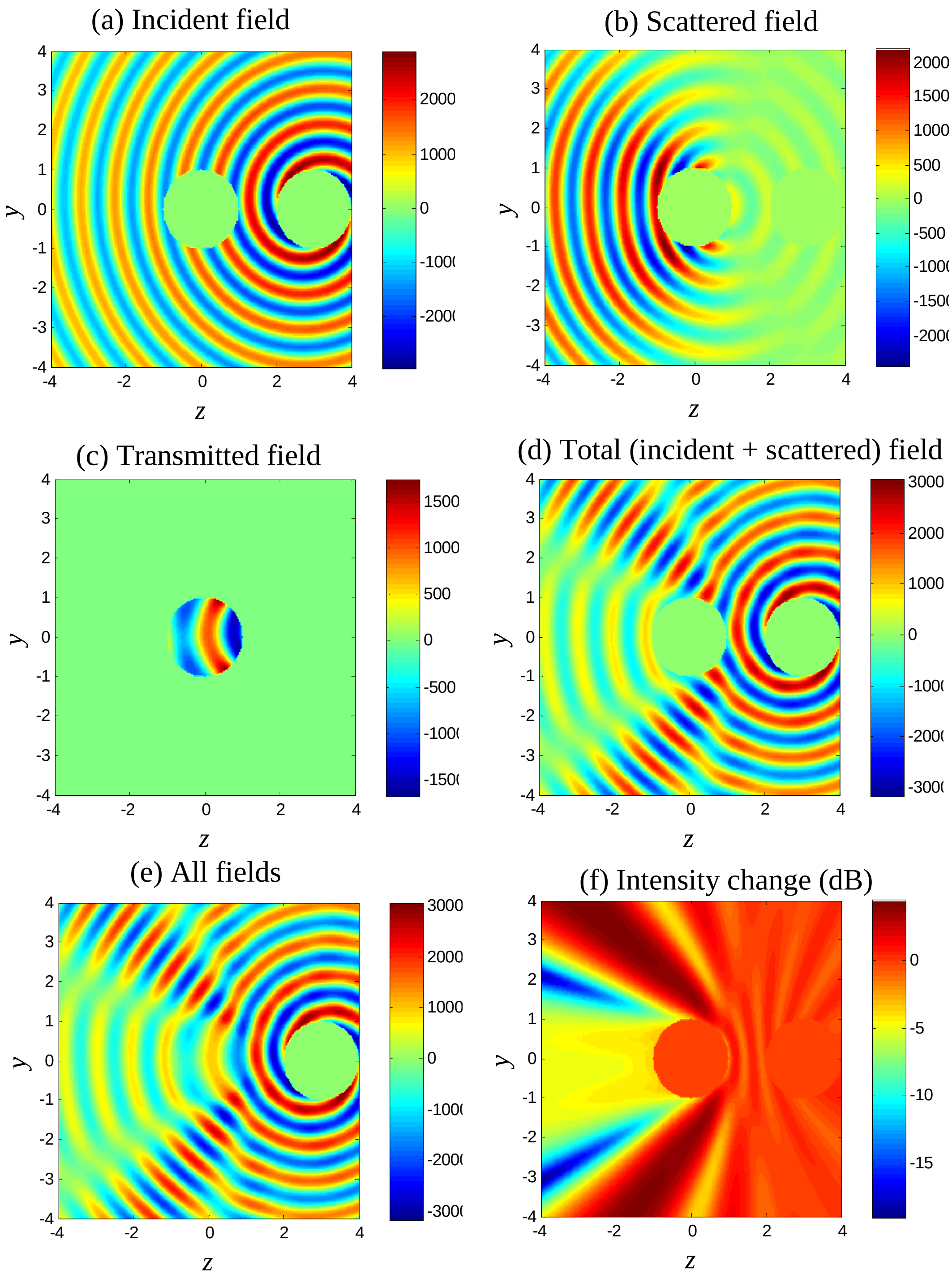

Figure 8. Prediction of diffraction on $z-y$ plane at acoustic wavenumber $k = 7.3$ and axial wavenumber $k_x = 1$. Conditions: $R_1 = R_2$=1 m; $S = 3$ m; M_1=0.8; a_1/a_∞=1.1; $M_\infty = 0$; $n = 2$. Results: (a) Incident field; (b) scattered field; (c) transmitted field; (d) total (incident+scattered) field; (e) all fields; (f) intensity ratio of total field to incident field (decibels).

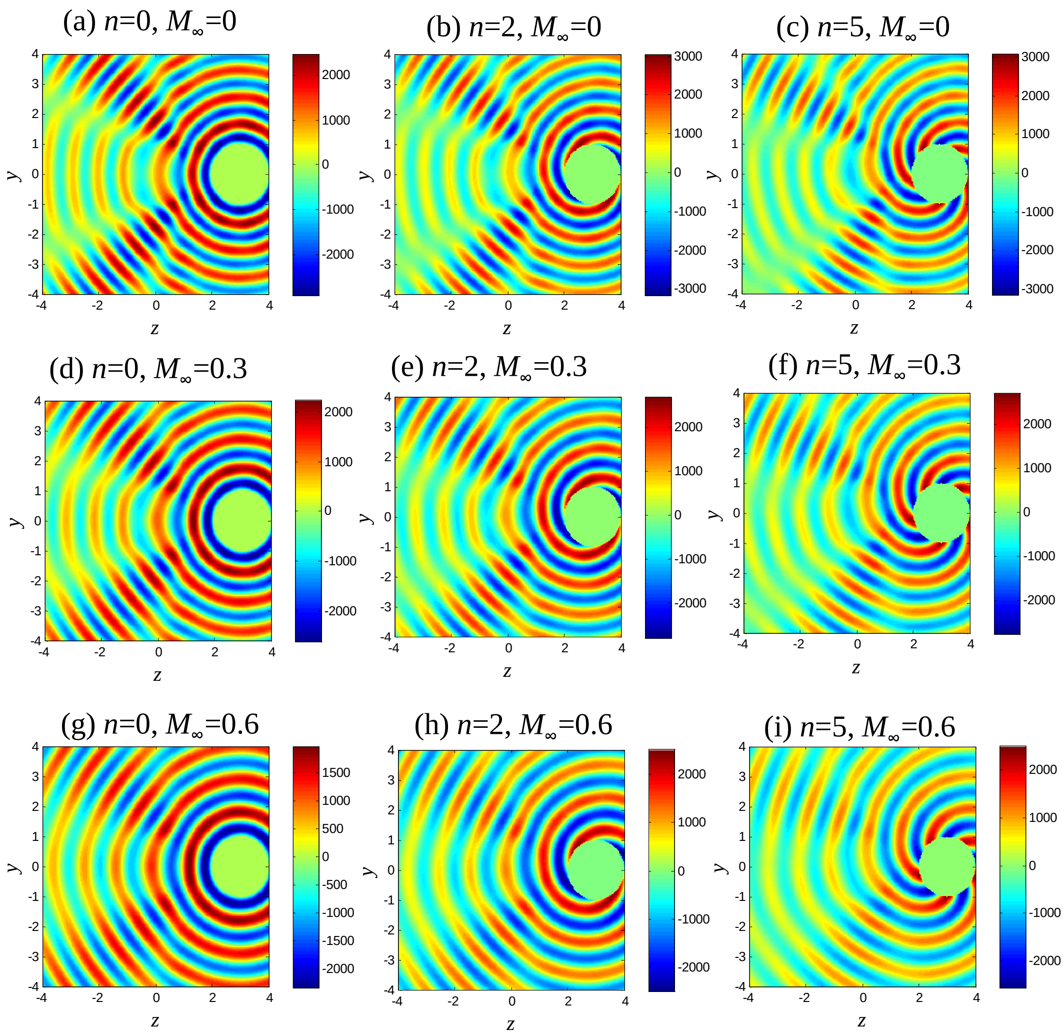

Figure 9. Impacts of azimuthal mode n and ambient Mach number M_∞ on the diffraction pattern for the setup of Fig. 8. (a) $n = 0, M_\infty = 0$; **(b)** $n = 2, M_\infty = 0$; **(c)** $n = 5, M_\infty = 0$; **(d)** $n = 0, M_\infty = 0.3$; **(e)** $n = 2, M_\infty = 0.3$; **(f)** $n = 5, M_\infty = 0.3$; **(g)** $n = 0, M_\infty = 0.6$; **(h)** $n = 2, M_\infty = 0.6$; **(i)** $n = 5, M_\infty = 0.6$.

B. Comparison with Experimental Data

We now consider the full solution (Eq. 31) with application to the experiment of SAS. In those experiments the jets had an exit diameter of 0.0445 m and the acoustic measurements were done at a distance R_o=3.1 m from the center of the scattering jet. The non-dimensional observer distance was $R_o/R = 137$. One drawback of the SAS study is that the ΔSPL was based on 1/3-octave spectra (not the narrowband spectra), which may introduce some smoothing effects, particularly at high frequency.

For our comparisons we select the jets at Mach number $M = 0.94$ and ambient total temperature ($T_0 = 293^o$ K) with spacings $S/R = 16.1$ and 11.0. SAS published results for jet Strouhal numbers $Sr = 2fR/U$=0.59 and 2.97. Their report does not provide sufficient data for the far-field spectra, so the spectra were generated using the ANOPP prediction method.[19] The parameterization of the Mach 0.94 jet for the aforementioned Strouhal numbers is shown in Fig. 10. Each sub-figure shows the wavepacket shape and the far-field intensity polar distributions. The modeled polar distribution of the far-field intensity is in excellent agreement with the ANOPP results (denoted as EXP). The azimuthal modes are $n = 1$ for $Sr = 0.59$ and $n = 5$ for $Sr = 2.59$. This trend is consistent with the finding of Papamoschou[18] that the azimuthal-mode number increases with increasing frequency. We note that the aft arc is dominated by the wavepacket noise source (the monopole contribution is insignificant there) so the scattering predictions use only the wavepacket radiated field.

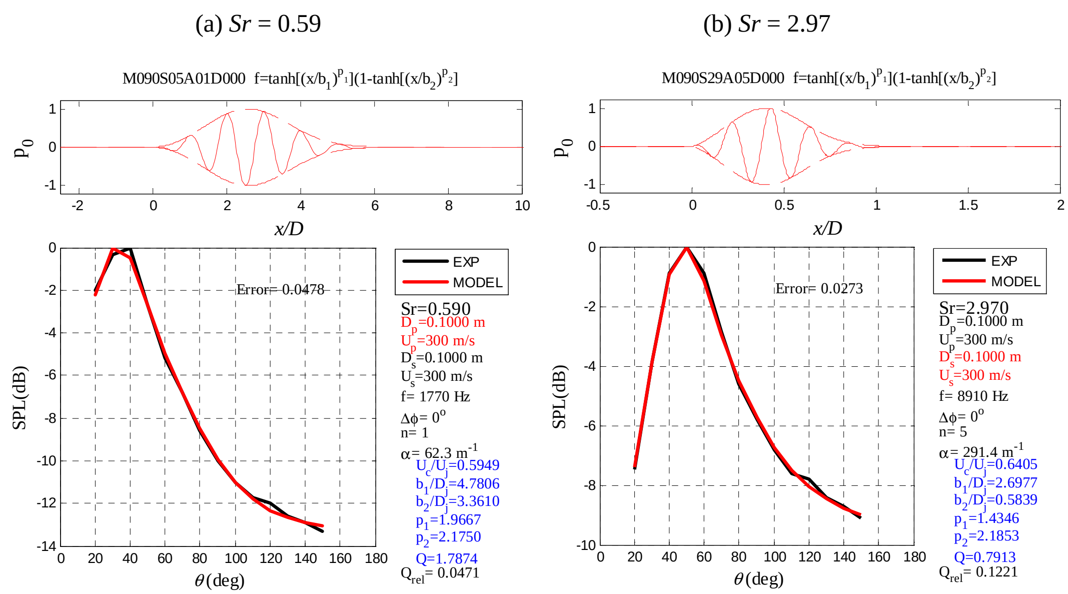

Figure 10. Parameterization and far-field intensity distribution of $M = 0.94$ cold jet. (a) Sr=0.59; (b) Sr=2.97.

Using the surface pressure distribution resulting from the parameterization, the scattering problem is solved according to the model of Section II. In constructing the solution for ΔSPL according to Eq. 34 we must account for the equal likelihood of azimuthal modes $+n$ and $-n$ in the jet. The fields of these modes are assumed to be uncorrelated. Therefore the process of Eq. 33 must be done separately for the $+n$ and $-n$ modes, then the intensities are added.

Figure 11 shows predictions of the azimuthal distribution of ΔSPL at $\theta_o = 40^o$ and compares with the experimental data (note that SAS used the single jet as a reference in the definition of ΔSPL, so their original results correspond to our ΔSPL+ 3 dB). At $Sr = 0.59$ the predictions match the experimental trends very well. The current prediction has better fidelity than the monopole-based model of SAS. The model captures the noise attenuation near $\phi_o = 90^o$, where shadowing occurs, and the amplification near $\phi_o = 50^o$. The latter is due to reflection of the incident field. Interference effects also contribute to the amplification and attenuation. At Sr=2.59 the agreement is fair, the prediction exhibiting oscillations versus ϕ_o that are not present in the experiment. We note that the randomness of the actual jet noise source, which is not included in our model, tends to smooth out oscillatory interference effects predicted using a deterministic harmonic source. Asymmetries in the distributions of Fig. 11 relate to the coordinate system being fixed to one of the jets and the finite observer distance relative to the jet spacing.

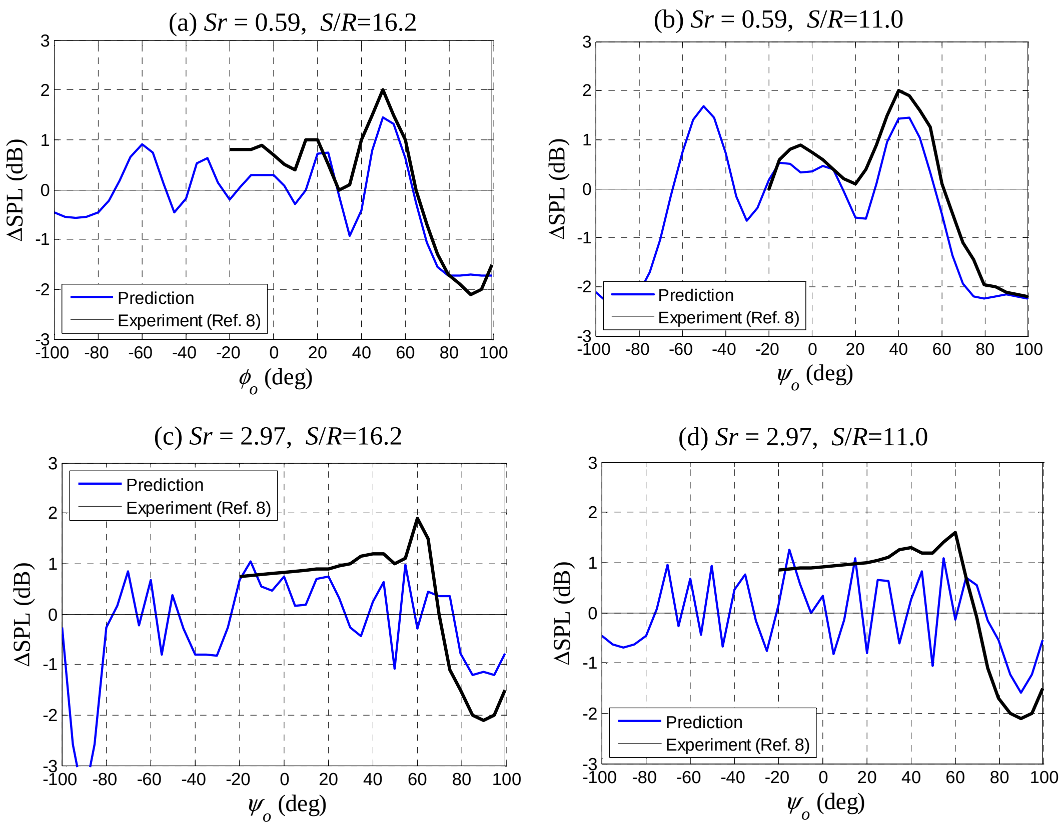

Figure 11. Comparison of model predictions of ΔSPL with the experimental data of Simonich et al.[9] Observer polar angle $\theta_o = 40^o$. (a) Sr=0.59, S/R=16.2; (b) Sr=0.59, S/R=11.0; (c) Sr=2.97, S/R=16.2; (d) Sr=2.97, S/R=11.0.

C. Application to HWB Configuration

As mentioned in the Introduction, the engines of the HWB are inherently close to each other. Review of the N2AEXTE model developed by Boeing, shown in Fig. 1, indicates an estimated spacing $S/R \approx 6$, with R the fan exit radius. The exhaust is composed primarily of the fan stream which operates at fan pressure ratios around 1.5, therefore the exhaust Mach number is around 0.8. The compression of the fan makes the stream moderately "warm" with $T_{0_1} = 330^o$ K. We use these values ($S/R = 6$, $M_1 = 0.8$, $T_{0_1} = 330^o$ K) in our predictive model for Strouhal numbers $Sr = 0.6$ and 1.0. The wavepacket is parameterized for the same exhaust conditions and Strouhal numbers. The results of the parameterization are shown in Fig. 12.

To present a comprehensive view of the effects of the scattering on noise we plot in Fig. 13 the ΔSPL, defined in Eq. 34, as isocontours on the azimuthal-polar (ψ_o-θ_o) observer plane. The observer distance is $R_o = 137R$ (same as in the SAS experiments). The patterns of Fig. 13 highlight the complexity of the jet-by-jet scattering. Generally speaking we get attenuation for $|\phi_o| \geq 60°$. The attenuation undulates with the polar angle, and for some polar angles the attenuation is so strong that the sound is less than that of the single isolated jet. This is the result of destructive interference between the incident and scattered fields. The amplification bands, resulting from reflection of the incident field, depend on frequency and occur typically for $20° < |\phi_o| < 50°$. The ΔSPL pattern becomes more complex with increasing frequency.

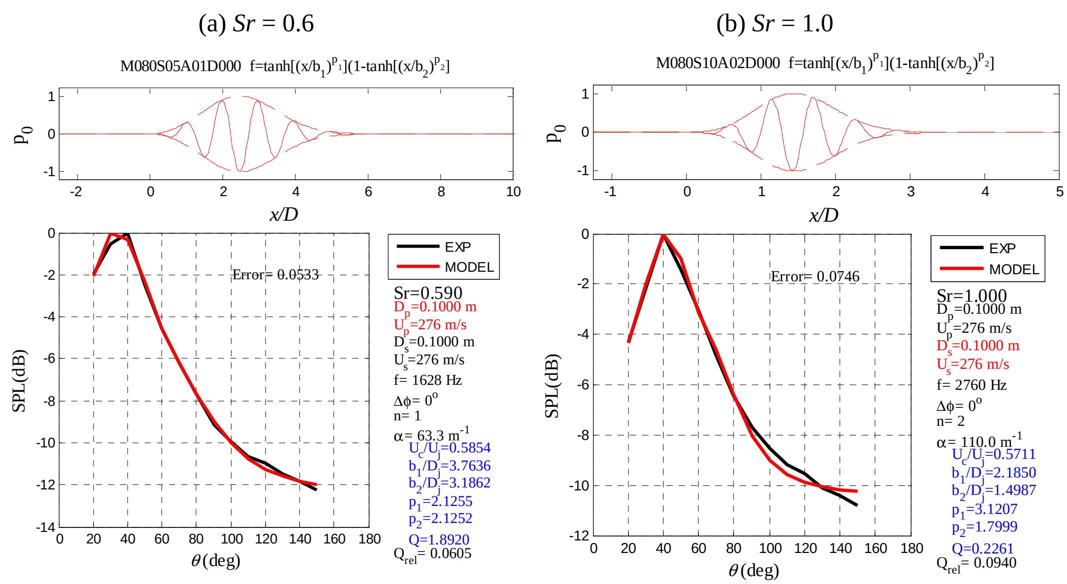

Figure 12. Parameterization and far-field intensity distribution of $M = 0.80$ jet simulating the fan stream of a large-bypass nozzle. (a) Sr=0.6; (b) Sr=1.0.

V. Conclusions

This report presented the development of an analytical model for the prediction of jet-by-jet scattering. The source jet is modeled as a radiating cylinder on which one can prescribe an arbitrary pressure (or acoustic potential) distribution. This treatment enables the incorporation of wavepacket sources that are becoming prominent in the simulation of jet noise. The scattering jet is modeled as an inviscid cylindrical interface with plug flow of variable Mach number and temperature. The ambient Mach number is also variable. The analysis solves the convective wave equation for the incident, scattered, and transmitted fields. The acoustic fields are Fourier-transformed in the axial directions and expanded into azimuthal Fourier modes. A central step in the analysis is shifting the pole of the incident field to the pole of the scattering cylinder through the use of the addition theorem for Bessel functions. With this shift all the fields are expressed as azimuthal Fourier series in a common coordinate system and the solution is readily obtained by applying the boundary conditions on the surface of the scattering cylinder. The prescribed pressure field on the radiating cylinder is parameterized to reproduce the experimental directivity of the far-field intensity of the isolated jet.

Cross-sectional contour plots of the acoustic field show that the scattering by the fluid interface of the jet

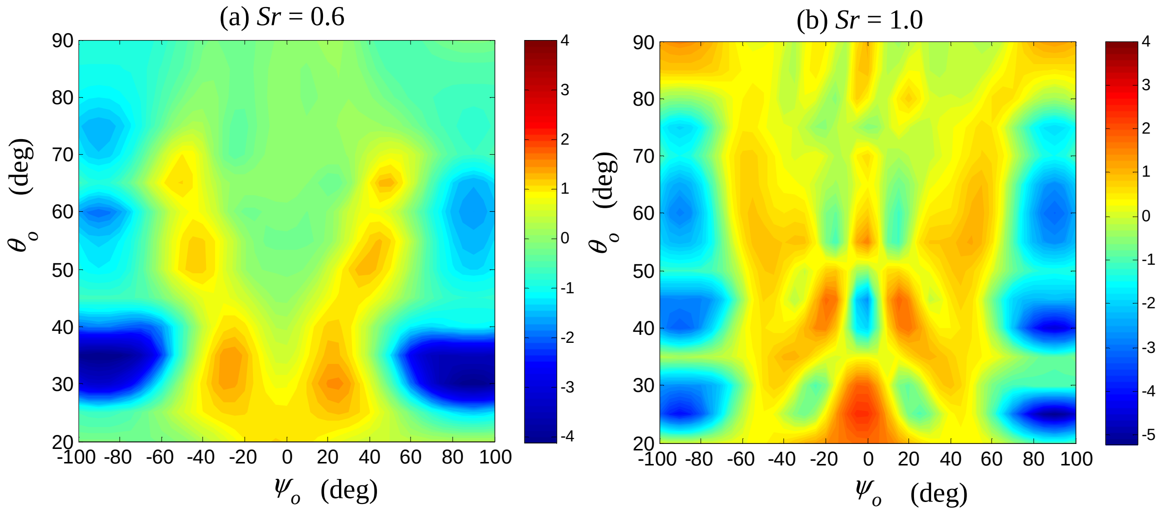

Figure 13. Maps of ΔSPL (dB) on the azimuthal-polar observer plane for jet spacing $S/R = 6$, typical of the HWB installation. (a) $Sr = 0.6$; (b) $Sr = 1.0$.

is a powerful phenomenon of similar magnitude as scattering from a solid cylinder. Regions of attenuation and amplification are identified. Comparison with available experimental data indicates that the model predicts the reduction and amplification trends with good agreement, its fidelity being better than those of past models that used a point source to simulate the jet noise.

Preliminary application to a typical jet configuration of the Hybrid-Wing-Body (HWB) airplane indicates a complex pattern of attenuation and amplification on the azimuthal-polar plane. This is bound to have an impact on the overall aircraft noise and particularly on the prediction of scattering around the elevon and vertical fins.

The present analysis does not include the effects of turbulence and jet spreading on the diffraction. Addition of these effects would entail a very complex computational model. Yet, despite its simplicity, the present model does a reasonable job in predicting the principal features of the acoustic field resulting by the interaction of the two jets.

Acknowledgement

The author is grateful for the support by NASA Contract NNL08AA00B, monitored by Dr. Casey Burley.

References

[1] Liebeck, R., "Design of the Blended Wing Body Subsonic Transport," *Journal of Aircraft*, Vol. 41, No. 1, 2004, pp. 10–25.

[2] Papamoschou, D. and Mayoral, S., "Jet Noise Shielding for Advanced Hybrid Wing-Body Configurations," AIAA 2011-912, Jan. 2011.

[3] Kantola, R., "Shielding Aspects of Heated Twin Jet Noise," AIAA 1977-1288, Oct. 1977.

[4] Bhat, W., "Acoustic Characteristics of Two Parallel Flow Jets," AIAA 1977-1290, Oct. 1977.

[5] Shivashankara, B. and Bhat, W., "Noise Characteristics of Two-parallel Jets of Unequal Flow," Jan. 1980.

[6] Gerhold, C., "Two-Dimensional Analytical Model of Twin Jet Shielding," *Journal of the Acoustical Society of America*, Vol. 69, No. 4, April 1980, pp. 904–908.

[7] Yu, J. and Fratello, D., "Measurement of Acoustic Shielding by a Turbulent Jet," *Journal of Sound and Vibration*, Vol. 98, No. 2, 1985, pp. 183–212.

[8] Lancey, T., "A Quadrupole Model for Jet Acoustical Shielding," *Journal of Sound and Vibration*, Vol. 279, No. 4, 1995, pp. 569–576.

[9] Simonich, J. C., Amiet, R. K., and Schlinker, R., "Jet Shielding of Jet Noise," NASA CR 3966, April 1986.

[10] Abramowitz, M. and Stegun, I. A., *Handbook of Mathematical Functions*, Dover, New York, 1965.

[11] Tam, C. and Burton, D., "Sound Generation by the Instability Waves of Supersonic Flows. Part 2. Axisymmetric Jets," *Journal of Fluid Mechanics*, Vol. 138, 1984, pp. 273–295.

[12] Crighton, D. and Huerre, P., "Shear-Layer Pressure Fluctuations and Superdirective Acoustic Sources," *Journal of Fluid Mechanics*, Vol. 220, 1990, pp. 355–368.

[13] Avital, E., Sandham, N., and Luo, K., "Mach Wave Radiation by Mixing Layers. Part I: Analysis of the Sound Field," *Theoretical and Computational Fluid Dynamics*, Vol. 12, 1998, pp. 73–90.

[14]Morris, P., "A Note on Noise Generation by Large Scale Turbulent Structures in Subsonic and Supersonic Jets," *International Journal of Aeroacoustics*, Vol. 8, No. 4, 2009, pp. 301–316.

[15]Reba, R., Narayanan, S., and Colonius, T., "Wave-Packet Models for Large-Scale Mixing Noise," *International Journal of Aeroacoustics*, Vol. 9, 2010, pp. 533–558.

[16]Papamoschou, D. and Mayoral, S., "Modeling of Jet Noise Sources and their Diffraction with Uniform Flow," AIAA 51st Aerospace Sciences Meeting, Jan. 2013.

[17]Papamoschou, D., "Prediction of Jet Noise Shielding," AIAA 2010-0653, Jan. 2010.

[18]Papamoschou, D., "Wavepacket Modeling of the Jet Noise Source," AIAA 2011-2835, June 2011.

[19]Gillian, R., "Aircraft Noise Prediction Program User's Manual," NASA TM-84486, Jan. 1983.